Available online at www.sciencedirect.com
SCIENCE DIRECT
Precambrian Research 144 (2006) 278–296
Precambrian Research
www.elsevier.com/locate/precamres

Late Neoproterozoic, Ordovician and Carboniferous events recorded in monazites from southern-central Madagascar

A. Berger [a,*], E. Gnos [a], G. Schreurs [a], A. Fernandez [a,b], M. Rakotondrazafy [c]

[a] *Institut für Geologie, Universität Bern, Baltzerstrasse 1, 3012 Bern, Switzerland*
[b] *Euniversité Claude Bernard, Labortoire Dynamique de la Lithosphere, 43 Boulevard du 11 Novembre, F-69622 Villeurbane Cedex, France*
[c] *Department des Sciences de la Terre, Université de Antananarivo, Antananarivo, Madagascar*

Received 1 June 2004; received in revised form 4 November 2005; accepted 11 November 2005

Abstract

The evolution of the basement of southern Madagascar north and south of the Ranotsara shear zone was investigated using (U + Th)/Pb electron probe monazite age dating in combination with petrographic constraints. Several monazite grains show a stepwise progression of younger ages towards the rim indicating partial and complete resetting during tectonic, metamorphic and/or fluid events. The oldest ages, ranging from 630–2400 Ma, occur relatively rare in relic cores. A first, clear age-population is dated at 550–560 Ma. Most ages fall in two populations at 420–460 and 490–500 Ma, which in some samples overlap in error. We interprete these ages as dating low-pressure and high-temperature metamorphism. We have also clear evidence for Carboniferous (300–310 Ma) monazite overgrowth rims, which can not directly be related to macroscopic structures or metamorphic parageneses. In combination with literature data, we propose that the observed monazite age populations are related to Gondwana amalgamation and subsequent rifting events during the break up of Gondwana. Our study confirms that only the electron or ion microprobe yields sufficient spatial resolution to date individual shells of multiple zoned monazites in the polymetamorphic basement of Madagascar.

Keywords: Monazite dating; Granulites; Gondwana; Madagascar; Ordovician; Carboniferous

1. Introduction

Two thirds of Madagascar consists of Precambrian to Paleozoic polymetamorphic basement and magmatic rocks containing relics of Archean crust (Fig. 1; e.g., Tucker et al., 1999; Collins and Windley, 2002). Most basement rocks record multiple high-grade metamorphism under upper amphibolite to granulite facies conditions yielding recrystallization and crystallization ages between ∼2500 and ∼430 Ma (e.g., Bazot et al., 1971; Hottin, 1976; Nicollet, 1990a; Martelat et al., 1997, 2000; Tucker et al., 1999; Markl et al., 2000; Goncalves et al., 2003). The basement rocks in northern and central Madagascar are intruded by 820–720 Ma calc-alkaline granitoid and gabbroic intrusions (Fig. 1; Ashwal and Tucker, 1997; Handke et al., 1999; Tucker et al., 1999; Kröner et al., 2000). These plutonic rocks also intrude the upper greenschist to amphibolite facies Proterozoic metasedimentary rocks of the Itremo Group (Fernandez et al., 2003; Fernandez and Schreurs, 2003; Collins et al., 2003a). Syntectonic alkaline stratoid granites (north of Itremo Group) were dated by Paquette and Nédélec (1998) at 627 ± 2 to 633 ± 1 Ma and were interpreted as magmatism associated with post-collisional collapse.

580–520 Ma apparently undeformed alkaline granitoids clearly crosscut deformed rocks and are generally interpreted to mark the lower time limit of the exten-

* Corresponding author. Tel.: +41 31 6318493; fax: +41 31 6314843.
E-mail address: berger@geo.unibe.ch (A. Berger).

0301-9268/$ – see front matter © 2005 Elsevier B.V. All rights reserved.
doi:10.1016/j.precamres.2005.11.010

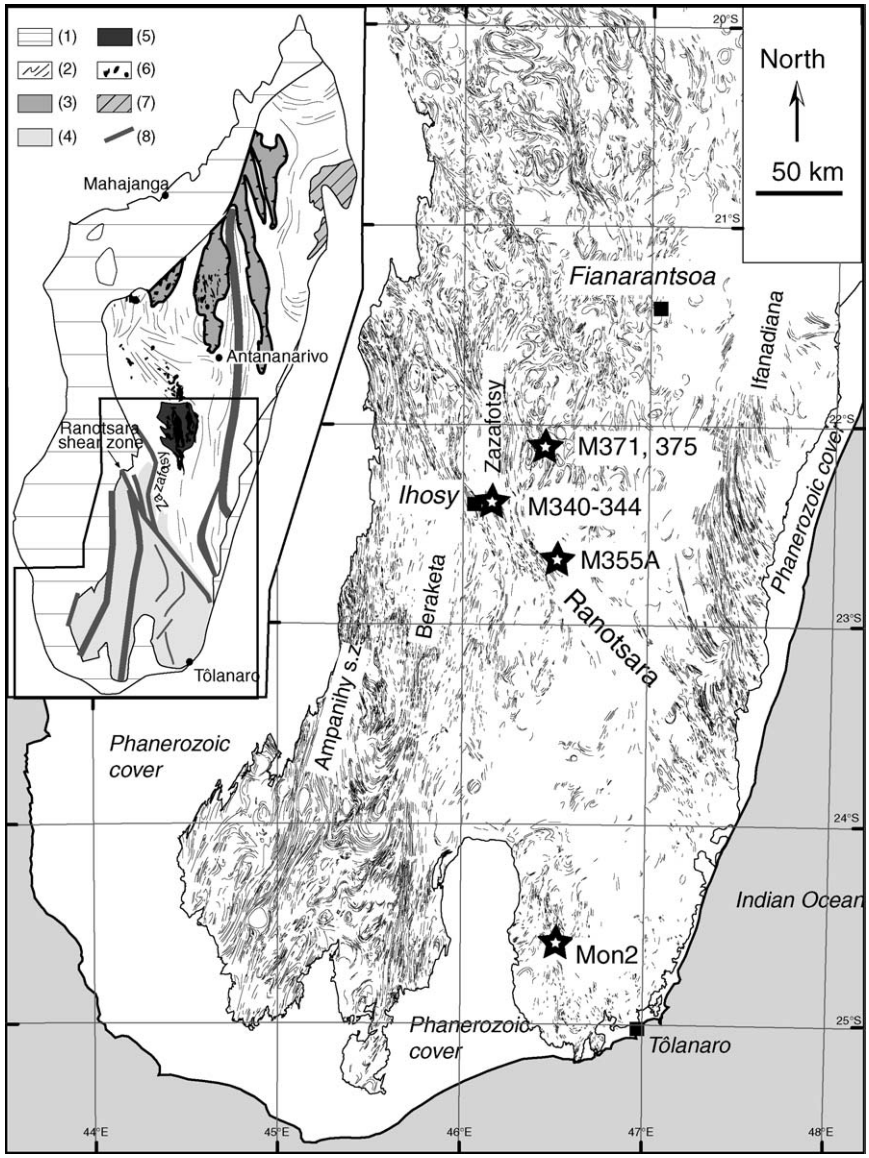

Fig. 1. Map of southern and central Madagascar with foliation traces in basement rocks, major shear zones (after Martelat, 1998) and location of samples. Foliation traces are derived from a georeferenced Landsat ETM+ mosaic with channels 741 in RGB. Contact between basement and Phanerozoic cover rocks is drawn using a georeferenced mosaic consisting of 1:100,000 geological maps. Inset shows a simplified tectonic overview of Madagascar, with (1) Phanerozoic cover; (2) Antananarivo block with main structural trends; (3) Tsaratanana thrust sheet; (4) Southern Madagascar (undifferentiated); (5) Itremo thrust sheet; (6) Middle Neoproterozoic (ca. 800 Ma) intrusive igneous rocks after Handke et al. (1997); (7) Antongil block; (8) Shear zones after Martelat (1998).

sive high-grade deformation (Ashwal and Tucker, 1997; Handke et al., 1997; Fernandez et al., 2003). However, different chemical and isotope age data indicate that metamorphic overprinting continued after 500 Ma (e.g., Martelat et al., 1997; Fernandez et al., 2003; Goncalves et al., 2003).

The basement of southern Madagascar is transected by several km-sized high-strain zones (Rolin, 1991; Windley et al., 1994; Martelat et al., 1999a; de Wit et al., 2001). All these shear zones show a steep foliation and a sub-horizontal to doubly plunging mineral lineation (Martelat et al., 1997) or intersection lineation. Stable isotope data record massive fluid flow inside the shear zones (Pili et al., 1997). One of the most striking high-strain zones is the NW-SE trending Ranotsara shear zone (Fig. 1). Originally, the Ranotsara shear zone was regarded as a major boundary separating a southern Archean block from the Proterozoic rocks to the north

(e.g., Windley et al., 1994). More recent studies suggest no major break across the Ranotsara shear zone (e.g., Martelat et al., 1999b; Markl et al., 2000). The fact that N–S striking shear zones show deflection at the Ranotsara shear zone led de Wit et al. (2001) to suggest that the latest ductile deformation along the Ranotsara high strain zone postdates movement along the N–S oriented shear zones.

The scope of our study is to reanalyze the previously documented garnet- and/or cordierite-bearing metapelites and associated rocks exposed south and north of the Ranotsara shear zone. These rocks are known to contain complexly-zoned zircons and monazites. We use monazite for dating because its mineral lattice is resistant to metamictization. Monazite in such old rocks yield precise chemical ages but is less refractive than zircon. It recrystallizes under presence of fluid and hence more likely records lower grade metamorphic events than zircon (e.g., Parrish, 1990; Foster et al., 2002). We also concentrated on dating small overgrowths that record the youngest history preserved in the monazite.

2. Methodology

We used polished thin sections and an electron microprobe for U–Th–Pb monazite dating, following the work of Ito et al. (1997) and Nicollet et al. (1997). Attempts to apply the more precise μ-XRF technique (Cheburkin et al., 1997) failed because the minimum spot size of 30 μm was not sufficient to resolve individual overgrowth shells. The microprobe allows for a spatial resolution of 1–2 μm, which is generally needed to date individual small overgrowth rims. Moreover, we used the complete monazite analysis technique (Scherrer et al., 2000) to have a better control on the liability of each single measurement point (e.g., if no other phases like oxides were analyzed), to have control that each analysis closes at 100 wt.%, and to see if systematic variations in monazite chemistry exist which can be correlated with metamorphic stages. High-contrast backscatter images were used to identify chemically variable zones before analysis. In each thin section we analyzed most of the monazite grains found. An age was subsequently calculated for each analysis following Montel et al. (1996). We used individual microprobe 2σ errors from counting statistics and error propagation (including errors on standards) for U, Th and Pb. The error on the individual age is largely controlled by the error on the Pb-measurement, which itself is influenced by the Th and U concentrations in the monazite.

To obtain individual age populations from the age data range of one sample the following procedure was used. A single spot age statistically defines a Gaussian curve with a half-width corresponding to the 1σ error. All spot ages obtained from one sample were used to construct a Gaussian sum-curve. The second derivate of this Gaussian sum curve allows us to determine different populations and their upper and lower bounds. In a second step a reduced χ^2 test is applied to find the best fit between the sum of the population peaks and the Gaussian sum curve. In the last step the area of the individual population Gaussians is set to one in order to obtain average errors for the population. All analyses can be done with the peak fitting module of the ORIGIN statistic software (Microcal Software Inc., 1999).

Age populations are tested for consistency with the isochron-method of Cocherie and Albarède (2001) and geological arguments. The measured Th–U–Pb ratio and errors were used to calculate a best fit through these data with Isoplot/Ex V.2 (Ludwig, 1999). The resulting isochrons are compared with the theoretically expected isochrons. Of course, if monazite-populations show only limited variation in Th/U ratios the data are not suitable for the isochron approach. The detected age populations are calculated using weighted mean and their related 2σ error (Ludwig, 1999). In these cases only a weighted mean average age is calculated. Analyses with ThO_2 contents <1 wt.% were discarded.

The following three data processing methods: (1) Gaussian sum curve; (2) isochron-method and (3) calculated error weighted mean, were combined as much as possible in order to test the consistency of each population. The quoted age of a population may be calculated by different methods as all the methods have advantages and disadvantages. The Gaussian-method is a purely statistical method and includes all data. This makes it independent from other information. However, the error propagation is complex. The isochron method gives the most robust result, because it can be tested by different decay systems. However, the method is only useful, when there is a certain spread in U/Th ratios. The error weighted mean of a specific population gives statistically the most useful value, but the detection of different populations has to be constrained by other methods.

In order to relate age information with metamorphic history, we analyzed the critical minerals using the electron microprobe. Cordierites, garnets and spinels were analyzed using 15 kV and 20 nA beam conditions and natural and synthetic silicate or oxide standards. Beam conditions of 25 kV and 50 nA and phosphate or REE-glass standards were used for the monazite analyses (Scherrer et al., 2000). Whole-rock chemical data on magmatic and metamagmatic rocks were obtained with standard XRF-technique.

3. Geological and structural description of the investigated area

Five of the studied samples (M340, M341, M342, M343, M344) are from a cordierite-bearing rock quarry located ca. 2 km east of Ihosy (22°24′17.2″S; 46°08′51.8″E). The geology of this quarry and another one, 4 km west of Ihosy, containing similar rock types, have previously been studied in detail (Nicollet, 1985, 1990a; Kröner et al., 1996; Nicollet et al., 1997; Ito et al., 1997; Markl et al., 2000; de Wit et al., 2001). In this area also mineralogical studies have been performed (e.g., Nicollet, 1990b). In the quarry east of Ihosy, two deformation phases (D1 and D2) can be distinguished, which are equivalent to those described by Martelat (1998) and Martelat et al. (2000). A first-phase foliation (S1) is characterized by compositional banding and planar arrangement of minerals. This foliation is isoclinally folded by N–S trending second-phase folds with subvertical axial planes dipping east and subhorizontal fold axes. Rootless second-phase folds and boudinaged leucosomes aligned within the subvertical main foliation indicate that transposition during D2 involved folding and boudinage of previously formed structures. Transposition during D2 resulted in a strong parallel orientation of S2 and S1 and the latter foliation can only be clearly distinguished from the former in hinge zones of second-phase folds. Sample M342 is a strongly foliated gneiss, that is interpreted as transposed layering resulting from D2 deformation. Pegmatoid pockets are often concentrated in D2 fold hinges suggesting that they formed syn-D2 (samples M341 and M343; de Wit et al., 2001). The occurrence of different fabric intensities (pegmatoid pockets, foliated gneisses) is characteristic for anatectic areas. This is caused by the variable melt volume and amount of melt segregation during deformation (e.g., Berger and Kalt, 1999). The investigated quarry is located within the N–S striking Zazafotsy shear zone that was interpreted as a D2 structure (Martelat, 1998). If one traces the second-phase axial plane foliations from the Ihosy quarry further south they are deflected into a NW-SE orientation in the Ranotsara shear zone (Fig. 1). The relative age relations of these two shear zones are not clear. The bending of a possible older foliation has been interpreted as a relative age criterion (Ranotsara postdates Zazafotsy; de Wit et al., 2001; Martelat et al., 2000) or as a strain gradient of conjugate systems during the same deformation event (Martelat, 1998). Sample M355A (22°38′10.6″S; 46°29′55.8″E) was taken within the Ranotsara shear zone. Its main foliation dips steeply and strikes NW-SE. Parallel trending brittle faults are common along the Ranotsara shear zone, which indicate several stages of deformation along this zone. The presence of pseudotachylites in this zone suggest deformation at ductile/brittle or brittle conditions. Furthermore, clay-dominated fault gouges indicate deformation at near surface conditions.

The area north of the Ranotsara shear zone and east of the Zazafotsy shear zone is dominated by large-scale, relatively open, N–S trending, second-phase folds with steep axial planes and subhorizontal fold axes (Fig. 2d). In some locations biotite-garnet-corundum bearing schists developed a S2 crenulation cleavage. Samples M371 and M375 are located in such an area (about 11 km northeast of the village of Zazafotsy: 22°07′51.8″S; 46°26′05.3″E), and contain a weakly-developed steeply E-dipping gneissic foliation. N–S striking steeply dipping brittle faults have also been observed in this area and seem to use the trends of pre-existing foliations. In addition, we investigate a cm-sized monazite from an alkaline pegmatite (Mon2) found south of the Ranotsara shear zone and northwest of the town of Tôlanaro (24°44′33.1″S and 46°51′52.0″E).

4. Sample description and monazite age populations

4.1. Samples from Ihosy quarry

4.1.1. Sample M340

Dark colored garnet-bearing biotite-plagioclase-gneiss. The rock is a foliated meta-monzonite dike, which intrudes the main metapelitic series (Fig. 2a). The chemical composition of the dike is poor in Si, but is strongly enriched in incompatible elements. The low Rb-content is in contrast to the strong enrichment in Sr. Ba-contents are in the range of granites (Fig. 3, Table 1). The rock consists mainly of biotite, feldspar, quartz and some rare resorbed garnet grains, which have a homogeneous composition (Table 2). The monazites have an irregular shape and occur as inclusions in all other main minerals. Most monazite grains have Th-contents below 0.5 wt.%, and are not suitable for chemical age dating. Only one grain with a Th-content of ∼3 wt.% yields a reliable error weighted mean of 537 ± 58 Ma (Tables 3 and 4).

4.1.2. Samples M341 and M343; coarse cordierite-gneiss

A detailed description for this medium-grained, pegmatoid lithology was given by Kröner et al. (1996) and Ito et al. (1997). Both samples are dominated by cordierite, biotite, potassic feldspar, plagioclase and quartz. Samples displaying pegmatoid textures are con-

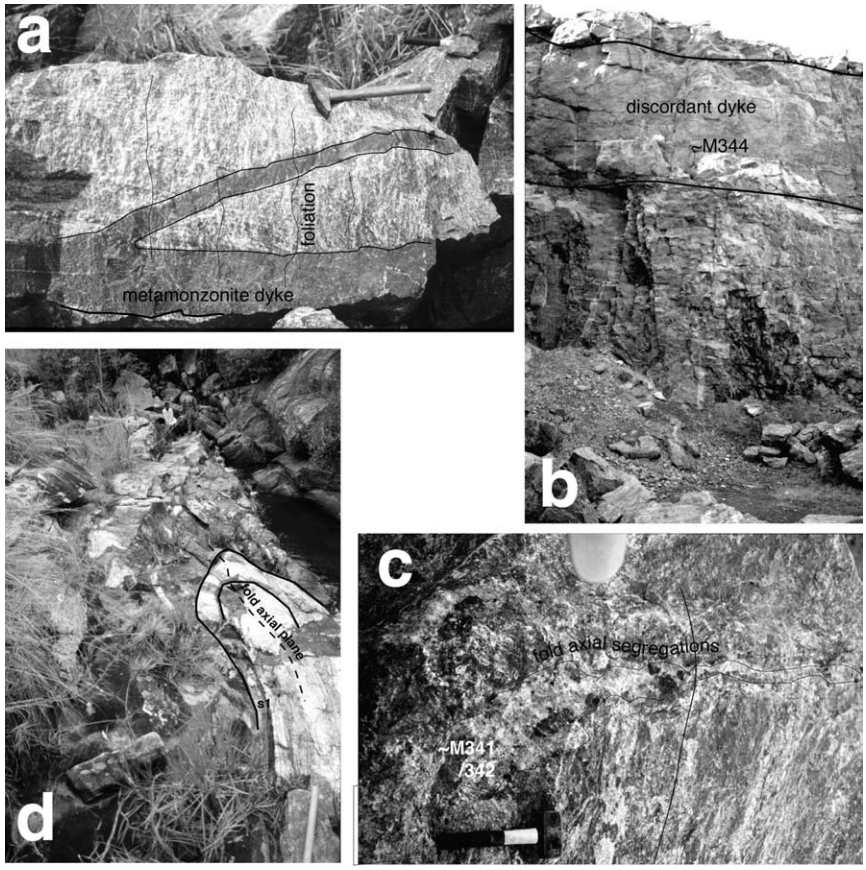

Fig. 2. Photographs showing field relationships (a) Ihosy quarry: strongly foliated cordierite-biotite-sillimanite-two feldspar-quartz gneiss crosscut by darker garnet-bearing metamonzonite dyke (equivalent sample M340). Note that both lithologies show high strain foliation; (b) Ihosy quarry wall showing early foliated metapelites and late post-deformation granite dyke (M344) intruding metapelites; (c) Ihosy quarry: fold hinge containing leucocratic segregations (outlined) with large crystals of cordierite and feldspar (M341-342); (d) isoclinal fold of compositional banding with vertical axial plane foliation in metasedimentary series (~10 km NE of Zazafotsy). Note person for scale.

centrated in fold hinges (see also de Wit et al., 2001, Fig. 2c and section on structures). The pegmatoid samples contain relative large (100 μm) monazites with a rounded and irregular shape. The main equilibration of monazite occurred at 457 ± 27 Ma (error weighted mean; Figs. 4 and 5), which is also well constrained by an isochron. However, a few spots yielded Carboniferous ages (Table 4).

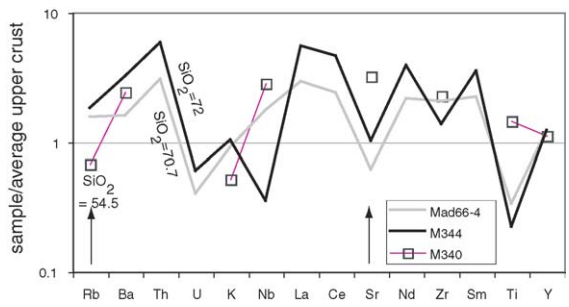

Fig. 3. Geochemistry of investigated magmatic and metamagmatic rocks (M340 to M344). The data are normalized to average upper crust (http//georef.org) in a geochemical ratio diagram. For comparison the granitic dyke of Kröner et al. (1996) is shown. Note the positive Sr-anomaly of the metamonzonite.

4.1.3. Sample M342

In contrast to samples M341 and M343, sample M342 is a strongly foliated gneiss, formed by aligned cordierite and locally recrystallized sillimanite. This sample contains small, block-shaped monazite, which dominantly give ages of 444 ± 23 Ma (error weighted mean). Two analyses show older monazite relics of 563 ± 40 and 1600 ± 14 Ma.

4.1.4. Sample M344

Unfoliated reddish biotite-bearing granite dike (Fig. 2b) crosscutting all foliated lithologies. This sample has an igneous texture with two feldspars, quartz and biotite. Some rare myrmikites have been detected.

Table 1
Whole rock chemistry of magmatic and metamagmatic rocks (measured by XRF)

Sample	M340	M344
SiO_2 wt.%	54.54	71.97
TiO_2 wt.%	1.86	0.32
Al_2O_3 wt.%	17.15	14.72
Fe_2O_3 wt.%	8.96	1.36
MnO wt.%	0.11	<0.01
MgO wt.%	2.94	0.71
CaO wt.%	4.29	1.48
Na_2O wt.%	4.35	2.63
K_2O wt.%	3.00	6.36
P_2O_5 wt.%	0.96	0.11
LOI wt.%	2.12	0.73
SUM wt.%	100.62	100.70
Ba ppm	1700	2115
Cr ppm	28	16
Cu ppm	12	14
Nb ppm	70	7
Ni ppm	32	17
Pb ppm	11	14
Rb ppm	74	203
Sr ppm	1125	382
Y ppm	24	27
Zn ppm	78	19
Zr ppm	542	298

The monazites are 50–100 μm large and commonly have an elongated shape. This granite itself is locally cut by cm-wide aplitic dikes. The chemistry of this granite is typical for anatectic granites and is basically identical with the analysis given in Kröner et al. (1996) (see also Fig. 3, Table 1). The error weighted average monazite age is 448 ± 19 Ma, but a few rims of Carboniferous age are also measured (Tables 3 and 4). The granite also contains rare older monazite relics (555 ± 61 Ma) interpreted as inherited grains during partial melting and melt segregation.

4.2. Samples from the Zazafotsy area

4.2.1. Samples M371 and M375

Both samples are weakly foliated, massive metamorphic rocks. Sample M371 is quartz-free and dominated by garnet, sillimanite, perthitic alkali-feldspar and large spinels. The high amounts of sillimanite and K-feldspar in combination with the absence of quartz point to a restitic composition developed during partial melting of a metapelite. Sample M375 is dominated by plagioclase and shows only a minor amount of alkali-feldspar. In both samples monazites not only occur in the matrix, but also in garnet, and even as inclusions in sillimanite. In many of the monazites 660 Ma and older monazite-relics (750–2400 Ma) are preserved. In garnets ~550 Ma old monazites are more frequent than in the matrix. Several spot ages belong to the 430 Ma population (Fig. 5). M371 is dominated by error weighted average mean populations of 559 ± 41, 418 ± 53 and 326 ± 58 Ma (Fig. 5), whereas M375 has main populations at 552 ± 50 and 455 ± 57 Ma (Gaussian technique). The latter sample also shows a reasonable spread in the U/Th ratio, which

Table 2
Characteristic electron microprobe analyses of metamorphic minerals

	Sample							
	M340 Meta-monzonite, garnet[b]	M340 Meta-monzonite, biotite[b]	M342 Meta-pelite, cord.[b]	M343 Meta-pelite, cord.[b]	M343 Meta-pelite, spinel[b]	M375 Meta-pelite, garnet[b]	M355A Restite, garnet[b]	M355A Restite, spinel[b]
SiO_2	36.87	35.04	48.92	47.73	bdl	38.53	38.19	0.29
TiO_2	bdl	4.42	bdl	bdl	0.05	bdl	0.05	bdl
Al_2O_3	22.10	16.6	34.62	34.33	57.1	22.54	22.89	58.86
Cr_2O_3	bdl	bdl	0.01	bdl	0.34	bdl	0.06	0.28
Fe_2O_3	2.16				3.69	1.14	2.25	3.53
FeO	29.49	18.15	6.56	5.84	31.68	27.92	26.1	28.13
MnO	3.28	0.14	0.15	0.05	0.25	0.55	0.27	0.06
MgO	5.51	11.06	9.82	10.12	5.29	9.33	10.32	8.76
ZnO	na	na	na	na	0.88	na	na	0.13
CaO	1.08	bdl	0.01	0.02	0.02	0.74	0.66	bdl
Na_2O	bdl	0.08	0.05	0.05	na	bdl	bdl	na
K_2O	bdl	10.05	bdl	bdl	na	bdl	bdl	na
H_2O[a]	–	3.84	–	–	–	–	–	–
Total	100.6	99.39	100.16	98.17	99.3	100.79	100.82	100.04

[a] Calculated; bdl: below detection limit; na: not analysed.
[b] Rock-type, mineral.

Table 3
Summary of age populations obtained by Gaussian sum curve analysis (Gauss), weighted mean and isochron-technique (isochron); n = number of analysis for the weighted mean of a single population

Sample	Comments	Population	Weighted mean	n	Iso-chron	Gauss
mon2	Single crystal	1	564 ± 7	8		554 ± 34
		2	482 ± 10	13		492 ± 15
M340	Meta-monzonite	1	537 ± 58	3		
		2	340 ± 60	4	340	
M341	Coarse cordierite gneiss	1	357 ± 10	10		
		2	457 ± 27	12	440	440
		3				420
		4				570
M342	Foliated cordierite gneiss	1	291 ± 68	4		322 ± 113
		2	444 ± 23	4		414 ± 52
		3				455 ± 52
M343	Coarse cordierite gneiss	1	490 ± 77	16		430 ± 28
		2	563 ± 73	7		541 ± 29
		3				367 ± 30
M344	Granitoid dyke	1	448 ± 19	18		
		2	339 ± 32 2 analysis at ∼550	7		
M355A	Garnet-feldspar gneiss	1				314 ± 30
		2	564 ± 7	7		557 ± 40
		3	455 ± 16	14	460	494 ± 29
M371	Restitic parts of partial molten metapelites (garnet, biotite, spinel)	1	261 ± 26	22		326 ± 58
		2	445 ± 62	8		418 ± 53
		3	561 ± 63	6		559 ± 41
M375		1	438 ± 98	7	430	455 ± 57
		2	550 ± 45	13	550	552 ± 50
		3	369 ± 150	9		357 ± 87
		4	404 ± 78	3		
		–	604–830	7		722 ± 44

The errors of the weighted mean and the Gauss-ages are related to 2 sigma.

allows the 550 and 430 Ma populations to be constrained by the isochron-method (Fig. 4).

4.3. Sample from the Ranotsara shear zone

4.3.1. Sample M355A

This sample is dominated by garnet and feldspars, whereas biotite is absent. The feldspars show pertithic exsolution lamellae and irregular patches characteristic of ternary feldspars. The garnets are up to 10 mm in size and coexist with sillimanite and hercynitic spinel. Spinel occurs as numerous inclusions in the core of the garnets and as larger grains in the matrix. Monazites are included in garnet and all other matrix minerals. Monazites included in garnet show the same age distribution as monazites in the matrix. Gaussian curve analysis clearly constrains three populations at about 557 ± 40, 494 ± 29 and 314 ± 30 Ma (Table 3). The isochron method well constrains a 460 Ma population (Fig. 4), giving a weighted mean age of 455 ± 16. This sample shows also clearly the young rims (Fig. 5).

4.4. Sample from north of Tôlanaro

4.4.1. Sample Mon2

Large, ∼5 cm-sized monazite single crystal from a REE pegmatite, which is located in the Anosyan mountains northwest of Fort Dauphin. The main rocks in the area are a granito-charnokitic basement. The granites are leucocratic and porphyritic rocks with oriented fabric. The sample itself is from the Manangotsy pass (24°44.331′S; 46°51.520′E). The pegmatite contains abundant dark brown, well crystallized monazites displaying a clear cleavage. The crystals are associated with large white apatite crystals, transparent to smoky quartz (locally forming veins or lenses)

Table 4
Microprobe U–Th–Pb concentrations and related ages

		Th	U	Pb	Pb err (%)	Age	Error
M340							
M7	3	36250	1818.3	1010	30.9	532.5	95.5
	4	37560	1593.6	1030	29.9	535.7	92.3
	5	27980	1478.4	810	38.4	548.8	122.4
	6	36540	1657.3	510	60.4	272.9	103.9
	7	37630	1523.3	690	45.1	362.3	99.9
	8	8970	1547.4	270	105.4	430.4	267.3
	9	26020	1495.5	290	106.2	211.3	143.9
	10	19620	1708.7	460	66.6	408.1	164.6
M341							
	1	62820	1471.8	1310	23.3	432.2	58.7
M1	2	58560	1627.3	1150	25.7	402.1	61
	3	52460	3079.4	1400	21.6	498.7	61.6
	2	53340	2746.2	1290	23.7	461.7	63.6
M3	1	54900	2390.6	1190	25.8	423.7	64.4
	3	54840	1740.8	1190	25.5	438.6	65.8
	1	50390	2746.9	1300	23.1	487.9	65.2
M5	2	52470	1439.4	1020	29	398.5	69
	3	53420	2475.9	1070	28.3	388.9	66.1
	1	51180	5904.1	1490	20.5	471.6	56
	2	59700	1693.1	1200	24.9	410.8	60
M4	3	61900	1155.1	1230	24.4	418	60
	4	55820	1967.2	1110	27.6	398.5	65.5
	5	56860	1683.4	1290	23.8	461.2	63.8
M6	1	53630	3565.2	1080	28.7	370.3	64.4
M342							
	1	8660	1718.5	380	78.1	590	262.8
M1	2	21080	1623.4	370	85.6	314.7	168.3
	3	32820	1680.8	730	41.5	425.5	106.4
	1	51360	2603.4	1050	29.9	392.1	70.2
M14	2	74550	1499.2	1670	18.6	468.5	49.1
	3	76040	953.8	1620	19.2	456.3	49.6
	4	118450	1139.7	2360	13.5	431	31.6
	1	54740	511.1	1140	26.3	450.7	69
	2	56890	703.3	1090	28.4	411.1	69.1
M1	3	55810	697.3	870	35.2	335	72
	4	65600	811.7	1050	29.2	344	60.6
	5	66630	888	1200	26.4	385.5	60.6
	6	65810	850.9	5210	5.1	1636.9	14.6
	1	14890	7995.9	600	50.9	330.1	104.7
M2	2	17340	7447	850	35.8	455.9	97.7
	3	17230	7037.4	1080	27.4	594.4	92.9
	4	13880	8079.6	850	33.8	471.3	95.1
M3	1	45260	4685.6	1100	28	406.3	67.7
	2	45280	6735.5	1360	22.5	451.3	59.5
M4	1	10400	6612.2	640	47.7	447.5	128.6
	3	13520	6300.9	660	46.3	433.3	121.2
M6	1	24740	3490.1	780	39.7	481.2	113.5
	2	25970	3395.7	620	48.1	374.8	110.2
	1	43650	5111.4	1120	27.2	415	67.3
M7	2	51040	4184.6	1270	24.8	438.2	63.9
	3	62920	841.4	1200	20	407.9	40

Table 4 (*Continued*)

		Th	U	Pb	Pb err (%)	Age	Error
	4	70000	735.7	1190	25.7	367.4	56.2
	5	59740	783	1140	26.6	408.6	64.1
	6	67350	545.3	1700	18	547	53.9
M12	2	14780	1476.3	290	99.2	332	202.5
	1	29260	3323.7	490	59.5	274.9	102.8
M11	2	24990	2509.2	430	68.9	291.2	125.7
	3	43100	2123.4	1300	23.5	577	76.3
M343							
	7	65190	933.2	1420	21.8	463.8	58
	8	64200	696.8	940	33.5	316.4	65
	9	65090	513.5	1460	21.4	487.1	59.2
	10	65140	643.4	1410	21.7	467.3	58
	11	66180	739.6	1340	23.7	435.7	60.1
M1	1	54740	511.1	1140	26.3	450.7	69
	2	56890	703.3	1090	28.4	411.1	69.1
	3	55810	697.3	870	35.2	335	72
	4	65600	811.7	1050	29.2	344	60.6
	5	66630	888	1200	26.4	385.5	60.6
	6	65810	850.9	5210	5.1	1636.9	14.6
	5	11730	8427.4	770	41.2	439.2	109.4
	6	15060	7845.3	1050	29.8	572	98.4
	7	11030	9039.9	500	62.1	279.6	109.9
M2	8	16470	7800.2	830	38	442.7	101.5
	9	11830	8657	880	35.5	489.3	103.3
	2	17340	7447	850	35.8	455.9	97.7
	3	17230	7037.4	1080	27.4	594.4	92.9
	4	13880	8079.6	850	33.8	471.3	95.1
M3	1	45260	4685.6	1100	28	406.3	67.7
	2	45280	6735.5	1360	22.5	451.3	59.5
	1	10400	6612.2	640	47.7	447.5	128.6
M4	2	9640	6665	600	50.1	428.1	129.7
	3	13520	6300.9	660	46.3	433.3	121.2
M6	1	24740	3490.1	780	39.7	481.2	113.5
	2	25970	3395.7	620	48.1	374.8	110.2
	1	43650	5111.4	1120	27.2	415	67.3
	2	51040	4184.6	1270	24.8	438.2	63.9
M7	4	70000	735.7	1190	25.7	367.4	56.2
	5	59740	783	1140	26.6	408.6	64.1
	6	67350	545.3	1700	18	547	53.9
M344							
	1	52990	968	1070	13.9	425.3	33.4
	2	47200	699	890	16.7	401.7	29.9
	3	47500	1047	980	15.0	429.5	33.0
	4	52210	920	1430	10.5	575.5	47.9
	5	68080	1123	1580	9.5	490.5	41.6
	6	49980	1408	850	17.7	348.4	25.6
M1	7	66870	847	1530	9.9	489.4	41.2
	8	46190	1692	990	14.8	427.3	33.1
	9	48850	1143	740	20.2	315.2	22.0
	10	60800	729	1130	13.4	399.4	31.7
	11	50060	838	1040	14.3	439.4	34.2
	12	52930	1068	880	16.8	348.9	26.0
	13	63850	1078	1600	9.4	528.3	44.9

Table 4 (*Continued*)

		Th	U	Pb	Pb err (%)	Age	Error
	1	49060	1172	1200	12.4	505.1	40.7
M2	2	49430	1470	780	19.4	322.0	22.9
	3	49270	1311	830	17.8	346.8	25.4
	4	50050	1248	950	15.5	392.1	29.9
M3	1	56810	994	1340	11.1	496.9	40.9
	2	62920	791	1190	12.9	405.7	32.4
		48690	728	1020	14.8	445.5	33.9
		48300	1016	1000	15.2	432.2	33.8
M4		47360	1040	960	15.5	422.1	32.8
		61550	878	1090	14.3	378.0	29.3
		52270	1279	990	15.6	391.9	30.3
		55730	1279	1270	11.8	472.5	39.3
M371							
	1	19180	1540.3	610	48.9	559.8	158.7
M1	2	18610	1262.4	300	107.7	296.2	199.6
	3	18760	1361.8	490	63.8	470.8	179.3
	4	18160	1504	390	76.8	378.3	177
	1	23570	1024.4	460	67.4	382.2	157.5
M7	2	22510	1058.2	320	97.5	276.6	169.8
	3	22230	749.2	420	71	380.5	164.6
	1	21420	1002.2	290	106.4	263.7	176.8
	2	21940	1100.3	320	96.8	281.3	171.1
M6	3	22370	998.7	600	50.8	520.9	155
	4	26720	782.9	740	42.7	561.8	139.5
	5	29500	712.8	570	56.3	400	137.3
	6	19460	789.3	300	105.1	305.1	199.9
M5	2	27410	770.4	630	50.6	469.3	141.8
	5	20630	975.1	490	66.1	458.9	182
	2	18050	1334.4	450	69.3	448.2	186.2
	3	16580	779.8	300	115.6	351.2	250.2
	4	16750	639.2	400	79.6	473.3	224
	5	17660	895.8	310	94.4	337.3	195.5
	6	20670	844.9	600	52	568.9	171.4
	7	19620	748.7	420	74.2	424.9	189.8
	8	19440	709.4	590	54.5	601.9	188.6
	10	27830	858.9	810	40.3	587.1	136.4
	11	17790	655.4	260	129.4	292.4	236.7
	12	17540	1466.3	300	114.3	301.7	215.1
M4	13	20080	1157.1	610	54.5	567.9	180.4
	14	27720	839.3	470	69.2	345.2	147.7
	15	14340	1277.9	240	125	291.2	225.2
	16	20410	1045.9	240	128.9	226.5	185.4
	17	17550	986.2	650	50.1	691.9	194.5
	18	17960	984.8	320	101.2	338.5	211
	19	23450	1074.8	480	64.5	397.9	155.6
	20	21360	982.4	760	44.7	684.4	172.7
	21	16530	1360	300	112.1	321	222.9
	22	13610	1430.6	270	125	331.3	254.7
	23	14360	1537.8	310	111.2	358.5	244.1
	24	14330	1457.9	380	83.3	444.4	220.8
M375							
	1	48140	5975.1	1320	42.6	435.9	109.9
M1	2	45270	5355.5	1580	37.7	559.2	120.4
	3	41750	1908.3	750	84	350	180.5
	4	37280	4134.6	1340	45	585.4	150.1

Table 4 (*Continued*)

		Th	U	Pb	Pb err (%)	Age	Error
	5	36960	3875.7	820	72	370.3	161.7
	6	51580	1862.6	1530	41.9	589.1	141
	7	53510	1815.6	1250	51.6	468.8	143.4
	8	47040	1739.1	920	70.7	390.1	167.4
	9	46110	1662.5	1000	70.2	433	183.9
	10	52970	1667.6	710	93.1	272.6	159.1
	11	53240	1706.6	1010	61.4	383.8	142.8
	12	47350	2268	1340	49.3	544.1	155
	13	49720	6099.4	960	68	309.8	130
	14	50190	5887.7	1270	54.7	409.2	134.7
	1	41750	3378.3	1220	59.4	514.5	179
	2	41690	3248.6	1190	58.6	506.7	174
	4	48240	3284.8	1450	47.9	546.6	150.9
	5	57220	3872.1	2190	32.1	692.8	120.4
M2	6	54100	4433.5	1260	63.7	410.7	158.5
	7	53790	3614.6	1560	47.2	529.1	144.8
	8	55960	3536.7	1840	39	604.5	132.4
	9	45290	1695.5	1580	50.6	687.9	195.5
	11	36770	1556.4	1040	68.5	552.3	216.2
	12	35020	5722.8	1390	59.1	574.1	195.3
	1	24330	4931.6	630	116.2	350	244.4
M3	2	20580	4885.2	970	77.4	588.3	256.7
	3	39890	5385.1	2180	37.9	830.9	166.8
	1	76680	2171.4	2880	27.6	759.4	110.6
M4	3	86300	1896.5	1340	57.5	324.3	114
	4	93310	2541	1960	42	430.5	106.5
	1	36100	5808.9	1240	73.8	501.5	217.6
M5	2	37620	7463.3	1490	54.1	534.3	165.4
	3	59870	5092.5	1820	49.4	529.3	151.4
	4	33740	4947.4	1560	53.6	689.6	201.3
Mon2							
	1	118570	1899.3	2730	11.9	487.4	30.5
	2	118190	2040.6	2800	11.5	499.3	30.1
	3	117600	1992.8	2790	11.7	500.6	30.7
	4	116950	1985.2	2780	11.7	501.5	30.8
	5	118020	2111.3	2840	11.5	506.2	30.2
	6	116610	2086.4	2510	12.9	453.4	31.7
	7	117130	2194.5	2790	11.8	499.8	30.8
	8	116940	2275.2	2880	11.3	515.4	30.1
	9	118220	1840.5	2650	12.3	475.4	31
	10	119010	1987.7	3210	10.4	568.5	29.4
	11	114570	1823.8	2710	12.2	500.7	32
	12	118340	2270.1	2710	12.2	480.1	31.1
	13	118960	2107.9	2720	12.1	481.5	30.8
	14	118540	1959.4	2850	11.5	507.9	30.4
	15	118320	1920.2	2680	12.3	479.2	31.4
	16	118200	2060.6	2930	11	521.9	29.4
	17	118440	2219.7	2800	11.6	496.1	30.1
	18	118190	2170.6	2760	11.8	490.6	30.5
	19	117610	2122.8	2960	11.1	528.8	30.1
	20	117350	2193.7	2650	12.3	474.3	31.1
	21	118820	1938.4	3180	10.3	564.8	247
	22	117710	2042.4	3080	10.7	550.6	250.2
	23	117050	2134.8	2920	11.2	523.9	224

Table 4 (*Continued*)

	Th	U	Pb	Pb err (%)	Age	Error
M355A						
	37750	3362.9	1300	12.0	591.8	58.7
	43490	5142.0	790	19.5	294.6	58.2
	45820	2453.5	1010	15.3	419.1	59.4
	61000	2388.4	1450	10.8	469.7	59.6
	54060	1133.6	1190	12.7	459.4	59.0
	53180	1216.8	740	21.6	290.1	59.4
	79150	2942.5	1920	8.2	481.9	59.6
	81800	2692.8	2020	7.8	496.6	59.0
	83540	2696.5	1930	8.1	465.9	59.3
	41320	1709.9	1080	14.1	512.5	59.9
	41440	1699.5	1050	15.0	497.7	61.7
	50980	1754.8	1110	13.6	436.8	59.3
	37200	3534.9	920	16.9	421.8	58.8
	50350	1657.1	890	17.4	357.1	59.3
	42530	4435.5	1140	13.6	446.4	59.6
	35080	1412.6	760	19.7	427.5	58.2
	29120	634.2	780	19.7	556.0	58.2
	74100	2200.8	1590	10.0	436.5	58.7
	55200	1289.5	1380	11.3	517.0	59.4
	54400	1072.4	1100	14.0	424.0	59.1
	73270	2513.8	1660	9.6	454.3	59.3
	74950	2517.7	1530	10.4	410.8	59.6
	30510	2479.2	1030	14.7	592.0	59.7
	31300	3116.3	920	16.6	494.2	318.5
	38080	1941.7	1130	13.8	565.1	298.8
	41490	1719.3	930	16.2	440.6	316.5
	33650	1507.8	690	21.7	399.7	331.2
	36340	908.0	950	16.6	537.6	0.1
	40380	923.3	990	17.5	507.9	0.1

Given errors are 2 sigma errors from the Pb-measurement.

and kaolinized feldspar. The selected crystal is inclusion free, except for small thorite inclusions. Two age populations are found. The core yields an age of 564 ± 7 Ma, whereas the large rim region gives an age of 482 ± 10 Ma. Using the Gaussian sum curve peak analysis method, the obtained populations are 554 ± 34 and 492 ± 15 Ma.

5. Monazite chemistry

One goal of this study was to find out if monazite chemistry can be linked with any known metamorphic stages. The petrography of our samples can be roughly subdivided into two stages (see next section), which have been previously described by several authors (e.g., Martelat, 1998; Markl et al., 2000). The background for this was provided, for example, by Förster (1998) and Pyle et al. (2001). In general, we see that if monazite becomes saturated in a brabantite component ($CaTh[PO_4]_2$), the amount of huttonite ($ThSiO_4$) starts to increase (Fig. 6a, Table 5). Moreover, the brabantite component also seems to drop slightly with increasing amount of huttonite. We also observe a negative correlation between huttonite component and Y-content (Fig. 6b). The Y-content is related to temperature, if buffered by garnet (Pyle et al., 2001).

In Fig. 6c the Th-content versus age relationship is shown. This diagram shows clearly that the obtained ages within the same sample are not linked with a specific Th content. The large monazite crystal Mon2 shows a 550 Ma core and a broad 480 Ma outer zone (Table 4). The crystal is chemically very homogenous (e.g., same huttonite component). This suggests that the crystal suffered diffusional Pb loss (e.g., Cherniak et al., 2004) at ~490 Ma rather than metamorphic recrystallization at different *P–T* conditions, which would not result in exactly the same monazite chemistry.

6. Petrology and metamorphism

Our samples come mainly from or direct north of the Ranotsara shear zone. Here different authors report *P–T*

Table 5
Selected electron microprobe analyses of monazites

	Sample						
	Mon02	Mon02	M341 M4[a]	M375 M2[a]	M371 M4[a]	M342 M14[a]	M343 M1[a]
	1[b]	10[b]	3[b]	9[b]	14[b]	4[b]	8[b]
P_2O_5	26.871	27.015	28.963	30.762	29.504	26.628	28.791
SiO_2	2.413	2.413	1.140	0.561	0.993	2.841	1.348
CaO	0.875	0.905	0.771	0.971	0.112	0.774	0.666
Y_2O_3	0.122	0.138	1.791	1.791	0.004	1.905	2.004
La_2O_3	14.488	14.248	13.727	14.885	15.063	10.276	13.642
Ce_2O_3	28.034	27.920	27.996	28.679	32.311	24.462	27.306
Pr_2O_3	2.912	2.913	3.134	3.077	3.704	3.067	3.167
Nd_2O_3	9.552	9.570	11.321	11.295	13.492	12.192	11.735
Sm_2O_3	1.090	1.092	1.702	1.905	1.516	2.084	1.808
Gd_2O_3	0.364	0.473	1.197	1.099	0.544	1.528	1.372
Tb_2O_3	0.026	0.000	0.110	0.153	0.017	0.146	0.084
Dy_2O_3	0.050	0.031	0.379	0.056	0.000	0.612	0.495
Ho_2O_3	bdl	bdl	0.027	0.262	0.000	0.038	0.056
Er_2O_3	0.009	0.021	0.132	0.255	bdl	0.137	0.161
Yb_2O_3	bdl	bdl	0.036	0.133	bdl	bdl	bdl
PbO	0.294	0.346	0.132	0.170	0.051	0.254	0.101
ThO_2	13.492	13.542	7.044	5.154	3.154	13.478	7.305
UO_2	0.215	0.225	0.131	0.192	0.095	0.129	0.079
Total	100.81	100.85	99.77	101.41	100.56	100.87	100.13
Si	0.386	0.385	0.179	0.086	0.155	0.452	0.212
P	3.641	3.652	3.857	3.974	3.901	3.588	3.827
$\sum$ T-site	4.028	4.037	4.037	4.060	4.056	4.040	4.039
Ca	0.150	0.155	0.130	0.159	0.019	0.132	0.112
Y	0.010	0.012	0.150	0.145	0.000	0.161	0.167
La	0.855	0.839	0.797	0.838	0.868	0.603	0.790
Ce	1.643	1.632	1.612	1.602	1.848	1.425	1.570
Pr	0.170	0.169	0.180	0.171	0.211	0.178	0.181
Nd	0.546	0.546	0.636	0.616	0.753	0.693	0.658
Sm	0.060	0.060	0.092	0.100	0.082	0.114	0.098
Gd	0.019	0.025	0.062	0.056	0.028	0.081	0.071
Tb	0.001	0.000	0.006	0.008	0.001	0.008	0.004
Dy	0.003	0.002	0.019	0.003		0.031	0.025
Ho			0.001	0.013		0.002	0.003
Er		0.001	0.006	0.012		0.007	0.008
Yb			0.002	0.006			
Pb	0.013	0.015	0.006	0.007	0.002	0.011	0.004
Th	0.491	0.492	0.252	0.179	0.112	0.488	0.261
U	0.008	0.008	0.005	0.007	0.003	0.005	0.003
$\sum$ A-site	3.970	3.956	3.958	3.922	3.926	3.982	3.956
Age (Ma)	487	568	418	772	379	431	316

The data are normalized to 24 charges.
[a] Grain.
[b] Analysis.

conditions in the range 800–950 °C and 0.7–0.9 GPa and a second, different metamorphism at 650–730 °C and 0.3–0.5 GPa (Fig. 7; Nicollet, 1988; Ackermand et al., 1989; Martelat, 1998; Martelat et al., 2000; Markl et al., 2000). These two metamorphic events are also related to garnet dominated paragenesis versus cordierite dominated paragenesis in metapelitic rocks (e.g., Martelat, 1998; Markl et al., 2000). We will refer to the two events as metamorphism I (garnet-dominated) and metamorphism II (cordierite dominated). The conditions reached

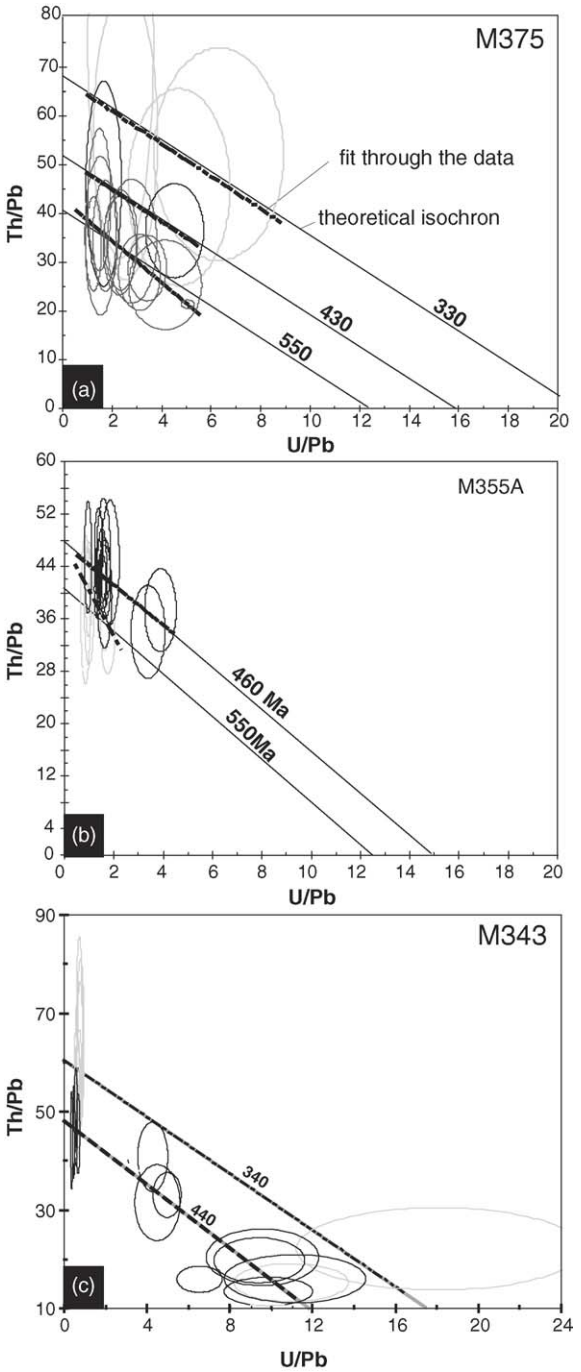

Fig. 4. Isochron-diagrams calculated with Isoplot (Ludwig, 1999). Bold-dashed lines represent the best-fit through the data and thin lines the expected isochron. (a) Sample M375: three isochrons can be constructed. (b) Sample M355A: 460 Ma isochron is well constrained, whereas the 550 Ma population shows a deviation from the theoretical isochron. (c) Sample M343: The 440 Ma isochron is well constrained and a 340 Ma isochron can also be constructed.

during metamorphism I are clearly located in the field of dehydration melting and responsible for the development of anatexites (e.g., Kröner et al., 1996). These are associated with restitic parts, which are widespread in southern Madagascar. Garnet is the dominant incongruent melting product at conditions of metamorphism I. Under the conditions of metamorphism II metapelites will be in the stability field of cordierite (e.g., Vielzeuf and Schmidt, 2001).

Samples M371, M375 and M355A contain large garnets + spinel (±secondary biotite). Sample M355A from the Ranotsara shear zone contains ternary feldspar characteristic for high-grade metapelites (located in the biotite dehydration melting field). In some samples (e.g., M371) hercynitic spinel + quartz are homogenously distributed in an equigranular matrix, but not observed in mutual contact. This is different to the development of microchemical domains during retrogression in migmatites (e.g., Kriegsman and Hensen, 1998). The experimental work of Das et al. (2001) suggests that this assemblage is restricted to temperatures >850 °C at intermediate pressure, conditions reached during metamorphism I. The conditions of the metamorphism II are still in the melting field, and local melt patches would have been produced from a fertile metapelitic protolith. However, restitic parts from earlier higher grade metamorphism would not be fertile anymore and only solid-state equilibration to produce cordierite at the expense of garnet would be probable.

Our samples from the Ihosy quarry show only cordierite + sillimanite (±resorbed garnet) assemblages, which can be correlated with our metamorphism II. The cordierites are intermediate in X_{Mg} (Table 2) and mineral zoning in the cordierite has not been detected. Mineral inclusions in cordierite or sillimanite show no evidence of a former metamorphic event. Some of the rocks (e.g., M342) show evidence that the gneissic structure contains cordierite, sillimanite and biotite. The latter grew during metamorphism II and most likely involved addition of H_2O and perhaps K_2O. The backreaction of restitic, dry composition may have occurred by infiltration of melt or aqueous fluid. The infiltration of melt would add K_2O but also more SiO_2 to the system. However, most investigated samples are poor in quartz, which make the infiltration of granitic melt unlikely. Therefore, the production of biotite is most likely related to infiltration of an aqueous fluid containing a certain amount of potassium. The observations can be correlated with other data from southern Madagascar, where Pili et al. (1997) inferred massive fluid flow along crustal shear zones.

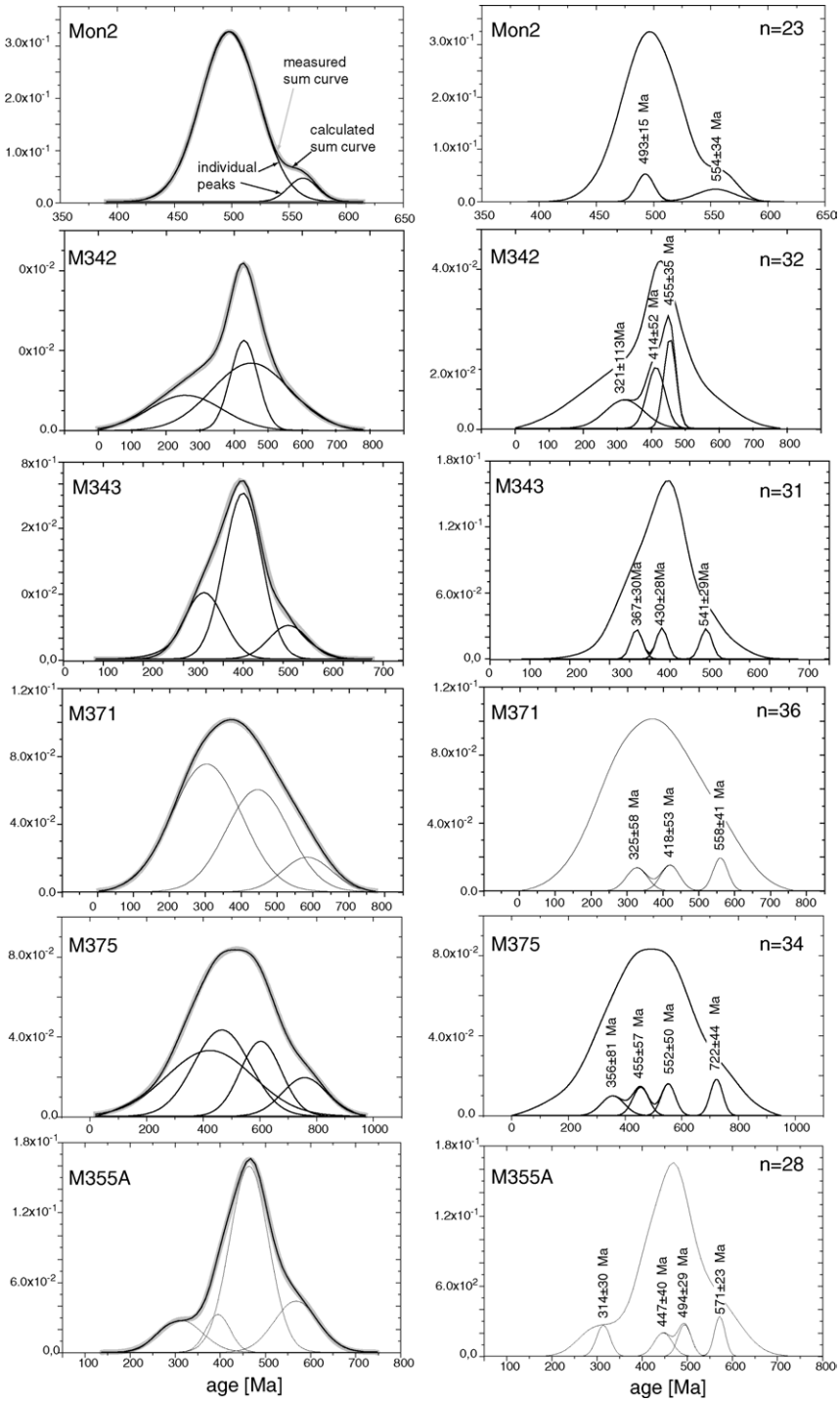

Fig. 5. Gaussian sum-curve analysis of the investigated samples: left diagrams show the Gaussian sum curve and the indiviudual population curves and grey shaded line is calculated sum curve. Right diagrams are the calculated sum-curve and the average population ages with their 2σ errors. Population ages are the same for the left diagrams. n = number of individual ages.

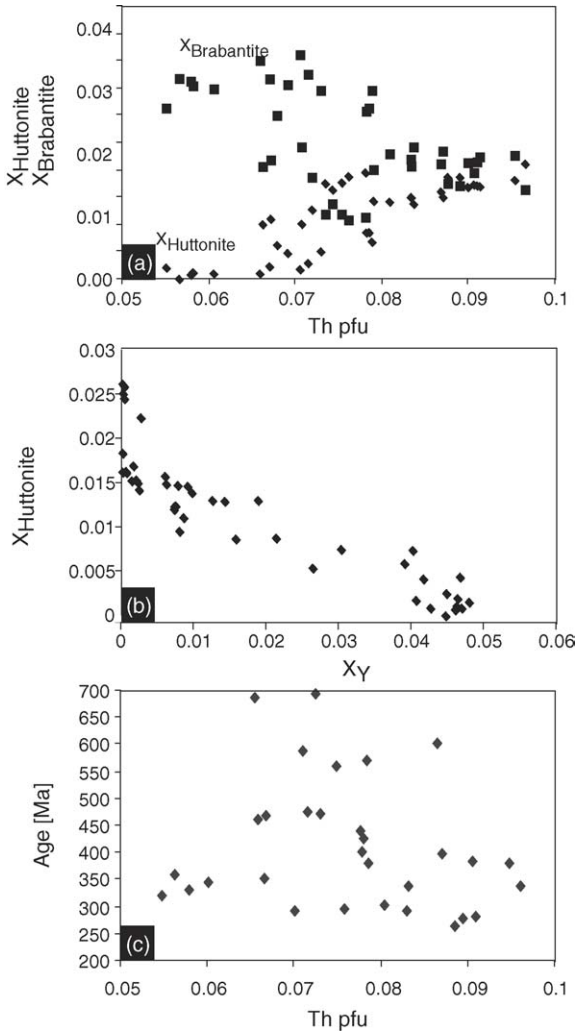

Fig. 6. Monazite compositions in sample M371. (a) Huttonite and brabantite component versus Th-contents of the monazites; (b) Huttonite component versus Y-content; (c) Th-content versus individual age. $X_{Huttonite}$, $X_{Brabantite}$ and $X_{Yttrium}$ component calculated after Pyle et al. (2001).

7. Discussion

7.1. Age populations

How well age populations can be recognized in a sample depends on the history of the rock, on the time distance between individual events recorded, and on the error associated with an individual age which is loosely related with the size of individual rims in complexly-zoned monazites. In situ methods have the additional advantage that a direct control allows us to determine whether ages from the inner part of the grain are equal or older than the rim regions. The large monazite (sample Mon2) clearly shows 2 cm-sized zones having ages of 492 ± 15 Ma and a 5 mm sized core of 554 ± 34 Ma (Gauss-populations; Fig. 5). Sample M355A shows in addition a clear 314 ± 30 Ma population although it is dominated by the 494 ± 29 and 557 ± 40 populations (Gauss-populations; Fig. 5). From these two samples it is clear that major geologic events took place at ~550–560, ~490–500 and ~300–310 Ma. In addition, the well-defined 460 Ma isochron of sample M355A (and other samples) can only represent a real age, because the same age at variable Th/U ratios demonstrates the growth of monazite at this time. This age is further constrained by looking at the Ihosy data where cordierite-dominated metapelitic rocks formed by replacement of garnet-dominated parageneses. The unfoliated granite M344 yields two well-defined populations, one at 448 ± 19 Ma, and an inherited population at 555 ± 61 Ma. All other cordierite-dominated samples also show dominant populations at 420–440 Ma (M341, M342 and 343). This shows that there exists a population at ~420–460 Ma.

7.2. The relation between ages, metamorphism and structures

The studied samples from southern Madagascar show the following age relationships: (1) The monzonitic dike (M340) intrudes the metapelite (M342) which contains inherited monazite and zircon grains. (2) Both rocks underwent metamorphism I, from which in our samples only resorbed garnets in M340 remain. Our garnet-dominated parageneses assigned to metamorphism I mainly preserve ages of 550 Ma, which are more widespread outside the Ihosy quarry. To this group belong our other samples collected north of the Ranotsara shear zone, as well as the large monazite from north of Tôlanaro. Although, these data suggest an age of 550 Ma for metamorphism I it remains open if the earlier of the two dominant deformation stages observed in Madagascar is correlated with this 550 Ma event, or if the deformation occurred at ~ 800 Ma or earlier (Fernandez et al., 2003; Collins et al., 2003b). (3) The deformed metapelites and metamonzonitic dikes at Ihosy are strongly affected by metamorphism II during which they become deformed again (steeply oriented N–S foliation) and a cordierite-sillimanite dominated paragenesis forms. The strongly foliated cordierite-rich gneiss contains coarse-grained pockets (in fold hinges) of less deformed but compositionally similar cordierite-rich material. The deformed cordierite-rich rocks are dominated by 410–460 Ma ages, and monazite data from one cordierite-bearing pocket (M343), where monazites contain large variations in Th/U ratio define a well-

constrained isochron at 440 Ma (Fig. 4, Tables 3 and 4). All data can be reconciled with formation of cordierite-rich parageneses (metamorphism II). As mentioned before, some reactions of metamorphism II are fluid consuming, which may also affected isotope systems in titanites (de Wit et al., 2001) and cause monazite overgrowth rims. (4) The S-type granite M344 post-dates deformation. The S-type character of this granite indicates, that partial melting of crustal material is the source of these melts, which would be consistent with metamorphism I and II. However, our discordant granite must be similar or younger than the cordierite-producing metamorphism, which have been related to 440 Ma. The commonly found to predominantly late Neoproterozoic (∼550 Ma) ages show that they were not completely erased by by younger tectonometamorphic events as 550 Ma ages are mainly found in zones where fluid flux is absent.

7.3. Comparison with previous studies

The investigation of monazite age populations in our study indicates four Neoproterozoic/Phanerozoic events. However, indications for the 550, 490, 440 and 300 Ma events are widespread in the literature. The study of Kröner et al. (1996) at Ihosy yielded metamorphic zircon ages of 557 ± 2.1 Ma in a granitic dike. Ito et al. (1997) dated monazites from the same quarry and obtained chemical monazite ages of 550 Ma and some older ages in inherited cores. Although numerous analyses at ∼440 and 490 Ma are listed in this contribution, the authors did not discuss their significance. More clear evidence for an Ordovician event is given by isotopic monazite ages of 481 ± 41 and 430 ± 32 Ma in rocks from the Ranotsara shear zone interpreted as reflecting ductile deformation during a late stage of collision tectonics (Nicollet et al., 1997). We similarly found the same age population in our sample M355A from the Ranotsara area. The fact that our sample contains few hydrous minerals is underlined by the dominant 550 Ma and older monazite ages obtained. Similarly, the two samples from the Zazafotsy area show a comparable pattern with 550 Ma and older ages dominating over 440 Ma ages. A foliated meta-monzonite (“granodiorite”) dike intruding the Ihosy quarry metapelites has been isotopically dated with U–Pb on monazite at 565 ± 15 Ma (Andriamarofahatra et al., 1990). Only one grain in our sample M340 from the same rock type contained sufficient Th to yield an age of 537 ± 58 Ma corroborating the result of Andriamarofahatra et al. (1990).

An undeformed granitic dike comparable with M344 was dated with zircon by Kröner et al. (1996) at 537 ± 5 Ma and also contained older inherited grains. Applying the same argumentation as Kröner et al. (1996) we conclude that the crystallization of dike M344 most likely occurred at 440 ± 19 Ma and that the 537 ± 5 Ma old zircons and the 550 ± 61 Ma monazite cores are inherited.

Paquette et al. (2003) reported a lower intercept at 300 Ma, and de Wit et al. (2001) at 266 ± 40 Ma. In addition, individual monazites ages of ∼300 Ma are known from Central Madagascar (Fernandez et al., 2003). As we paid special attention to obtain data from the rim regions, our data also allowed to demonstrate that a ∼300 Ma event is locally detectable.

7.4. Indication for the tectonic evolution

Monazite dating of metamorphic rocks from southern Madagascar reveals four monazite age populations. One at ∼550 Ma (Late Neoproterozoic), a second at ∼490 Ma (Ordovician) and a third at ∼440 Ma (Ordovician) has been detected. The latter two overlap in error in some samples and also isochron of 460 Ma are measured. A fourth population at ∼300 Ma (Carboniferous) can be distinguished unambiguously. In addition, monazite cores may preserve ages as old as 2400 Ma.

The ∼550 Ma ages are associated with granulite-facies metamorphism (metamorphism I: 850–950 °C ∼1.0 GPa). This high-grade metamorphic event is usually interpreted as the result of crustal thickening during Gondwana amalgamation (e.g., Tucker et al., 1999; Martelat et al., 1999a, 2000; Collins et al., 2003b). A main equilibration of monazite occurs in Ordovician times and is associated with low-pressure/high-temperature metamorphism characterized by formation of cordierite (metamorphism II: 650–730 °C and ∼0.5 GPa). This type of metamorphism seems to be in relation with the second ductile deformation event whose structures are consistent with E–W horizontal shortening in an overall sinistral transpressive regime. In some cases monazites included in cordierites, which are clearly aligned in the second phase foliation, date the cordierite-producing event at ∼440 Ma. However, the ∼490 Ma age population is also commonly found in association with second-phase ductile shear zones. Our data can be best reconciled if we propose that the shear zones formed at ∼490 Ma, and that they were reactivated at ∼440 Ma causing local transformation into cordierite-dominated assemblages. The youngest age population at ∼300 Ma can be related to late Carboniferous rifting. Evidence for intercratonic rifting is recorded in the Late Carboniferous/Early Permian sedimentary rocks that overly the basement along the

eastern margin of the Morandava basin (Fig. 1; Besairie, 1972).

The monazite age populations correspond closely to major geochronologic and chronostratigraphic boundaries: (1) Precambrian/Cambrian boundary (540 Ma); (2) Cambrian/Ordovician boundary (500 Ma); (3) Ordovician/Silurian boundary (435 Ma), and (4) Carboniferous/Permian boundary (295 Ma). There is general consensus that these boundaries reflect large scale plate reorganizations, and a link between monazite age populations and large-scale tectonic events is plausible. On a Gondwana scale the evolution of sedimentary basins record tectonic events which may be related to our age populations. The sedimentary basins of northwestern Australia, the basins of northern and western Africa (Bellini and Massa, 1980; Baldis et al., 1993; Borel and Stampfli, 2002) all show progressive marginal rifting of the platforms at ∼500 Ma following Gondwana amalgamation. In some of these basins a major unconformity is recorded at the Ordovician/Silurian boundary at ∼430 Ma (e.g., Bellini and Massa, 1980) probably related with subduction along parts of the Gondwana margin. Although rifting of Gondwana appears to have occurred in several steps since ∼500 Ma, break-up of Gondwana intensified in the Carboniferous at ∼300 Ma and reached its peak in the Mesozoic.

The importance of Ordovician and younger events recorded in Precambrian basement rocks of Madagascar which was situated in the core of Gondwana opens the possibility to study tectonic events in the absence of a contemporaneous sedimentary record.

Acknowledgements

The project was supported by Swiss National Science Foundation grants 2000-65306.01 and 21-26579.89. We thank one anonymous reviewer and Alan Collins for constructive comments. Jörg Giese is thanked for help in preparing Fig. 1.

References

Ackermand, D., Windley, B.F., Razafiniparany, A., 1989. The Precambrian mobile belt of southern Madagascar. In: Daly, J.S., Cliff, R.A., Yardley, B.W.D. (Eds.), Evolution of Metamorphic Belts. Geological Society Special Publication, pp. 293–296.

Andriamarofahatra, J., de la Boisse, H., Nicollet, C., 1990. Datation U–Pb sur monazites et zircons du dernier episode tectono-metamorphique granulitique majeur dans le sud-est de Madagascar. Comptes Rend. Acad. Sci. Series 2 (310), 1643–1648.

Ashwal, L.D., Tucker, R.D., 1997. Archaen to Neoproterozoic events in Madagascar: implications for the assembly of Gondwana. Terra Nova Abst. 9 (Suppl. 1), 163–164.

Baldis, B.A.J., Martínez, R.D., Pereyra, M.E., Pérez, A.M., Villegas, C.R., Martínez de Giménez, P., 1993. Upper proterozoic-lower paleozoic transgondwanic ruptures and events between North Africa and South America. In: Findlay, R.H., Unrug, R., Banks, M.R., Veevers, J.J. (Eds.), Gondwana Eight. Balkema, Rotterdam, pp. 23–27.

Besairie, H., 1972. Géologie de Madagascar: I. Les terrains sédimentaires. Annales Géologiques de Madagascar, Nr. XXXV, Antananarivo, Madagascar.

Bazot, G., Bousteyak, L., Hottin, G. and Razafiniparany, A., 1971. Carte du metamorphisme de Madagascar (with explanatory notes). Doc. Bur. Géol., Tananarive, Madagascar.

Bellini, E., Massa, D., 1980. A stratigraphic contribution to the Paleozoic of the southern basins in Lybia. In: Salem, M.J., Busremil, M.T. (Eds.), The geology of Lybia, vol. I. Academic Press, London, pp. 3–56.

Berger, A., Kalt, A., 1999. Structures and melt fractions as indicators of the rheology of cordierite bearing migmatites of the Bayerische Wald (Variscan belt, Germany). J. Petrol. 40, 1629–1639.

Borel, G.D., Stampfli, G.M., 2002. Geohistory of the North West Shelf: a tool to assess the Palaeozoic and Mesozoic motion of the Australian Plate. In: Proceeding of Petroleum Exploration Society of Australia Symposium, Keep, M., Moss, S.J. (Eds.), The sedimentary basins of Western Australia 3. Perth, pp. 119–128.

Cheburkin, A., Frei, R., Shottyk, W., 1997. An energy dispersive minprobe multielement analyzer (EMMA) for direct analysis of trace elements and chemical age dating of single mineral grains. Chem. Geol. 135, 75–87.

Cherniak, D.J., Watson, E.B., Grove, M., Harrison, T.M., 2004. Pb diffusion in monazite: a combined RBS/SIMS study. Geochim. Cosmochim. Acta 68, 829–840.

Cocherie, A., Albarède, F., 2001. An improved U–Th–Pb age calculation for electron microprobe dating of monazite. Geochem. Cosmochem. Acta 65, 4509–4522.

Collins, A.S., Johnson, S., Fitzsimons, I.C.W., Powell, C., Hulscher, B., Abello, J., Razakamanana, T., 2003a. Neoproterozoic deformation in central Madagascar; a structural section through part of the East African Orogen. In: Yoshida, M., Windley Brian, F., Dasgupta, S. (Eds.), Proterozoic East Gondwana; Supercontinent Assembly and Breakup. Geological Society of London.

Collins, A.S., Fitzsimons, I.C.W., Hulscher, B., Razakamanana, T., 2003b. Structure of the eastern margin of the East African Orogen in central Madagascar. Precamb. Res. 123, 111–133.

Collins, A.S., Windley, B.F., 2002. The tectonic evolution of central and northern Madagascar and its place in the final assembly of Gondwana. J. Geol. 110, 325–339.

Das, K., Dasgupta, S., Miura, H., 2001. Stability of osumilite coexisting with spinel solid solutions in metapelitic granulites at high oxygen fugacity. Am. Mineral. 86, 1423–1434.

de Wit, M.J., Bowring, S.A., Ashwal, L.D., Randrianasolo, L.G., Morel, V.P.I., Rambeloson, R.A., 2001. Age and tectonic evolution of neoproterozoic ductile shear zones in southwestern Madagascar, with implications for Gondwana studies. Tectonics 20, 1–45.

Fernandez, A., Huber, S., Schreurs, G., Villa, I.M., Rakotondrazafy, M., 2003. Age constraints on the tectonic evolution of the Itremo region in Central Madagascar. Precamb. Res. 123, 87–110.

Fernandez, A., Schreurs, G., 2003. Tectonic evolution of the Proterozoic Itremo Group metasediments in central Madagascar. In: Yoshida, M., Windley, B.F., Dasgupta, S. (Eds.), Proterozoic East Gondwana: Supercontinent Assembly and Breakup, Geol. Soc. Lond. Spec. Publ. 206, pp. 381–399.

Foster, G., Gibson, H.D., Parrish, R., Horstwood, M., Fraser, J., Tindle, A., 2002. Textural, chemical and isotopic insights into the nature and behaviour of metamorphic monazite. Chem. Geol. 191, 183–207.

Förster, H.J., 1998. The chemical composition of REE-Y-Th-U-rich accessory minerals in peraluminous granites of the Erzgebirge-Fichtelgebirge region, Germany, Part I: The monazite-(Ce)-brabantite solid solution series. Am. Mineral. 83, 259–272.

Goncalves, P., Nicollet, C., Lardeaux, J.M., 2003. Finite strain pattern in Andriamena Unit (North-Central madagascar), evidence for Late-Neoproterozoic-Cambrian thrusting during continental convergence. Precamb. Res. 123, 135–157.

Handke, M.J., Tucker, R.D., Hamilton, M.A., 1997. Age, geochemistry, and petrogenesis of the Early Neoproterozoic (800–790 Ma) intrusive rocks of the Itremo Region, Central Madagascar. In: Cox, R., Ashwal, L.D. (Eds.), Gondwana Res. Group Misc. Publ. 2, pp. 28–29.

Handke, M.J., Tucker, R.D., Ashawal, L.D., 1999. Neoproterozoic continental arc magmatism in west-central Madagascar. Geology 27, 351–354.

Hottin, G., 1976. Presentation et essai d'interpretation du Precambrien de Madagascar. Bull. Bur. Res. Geol. Min. France Série 2 (4), 117–153.

Ito, M., Suzuki, K., Yogo, S., 1997. Cambrian granulite to upper amphibolite facies meta-morphism of post-797 Ma sediments in Madagascar. J. Earth Planet. Sci. Nagoya Univ. 44, 89–102.

Kriegsman, L.M., Hensen, B.J., 1998. Back reaction between restite and melt: Implications for geothermobarometry and pressure temperature paths. Geology 26, 1111–1114.

Kröner, A., Braun, I., Jaeckel, P., 1996. Zircon geochronology of anatectic melts and residues from a high-grade pelitic assemblage at Ihosy, southern Madagascar: evidence for Pan-African granulite metamorphism. Geol. Mag. 133, 311–323.

Kröner, A., Hegner, E., Collins, A.S., Windley, B.F., Brewer, T.S., Razakamanana, T., Pidgeon, R.T., 2000. Age and magmatic history of the Antananarivo block, central Madagascar, as derived from zircon geochronology and Nd isotopic systematics. Am. J. Sci. 300, 251–288.

Ludwig, K.R., 1999. Users manual for ISOPLOT-EX, version 2. Geochronological tool kit for Microsoft Excel. Berkley Geochronological Center Spec. Publ., 1A.

Markl, G., Bäuerle, J., Grujic, D., 2000. Metamorphic evolution of Pan-african granulite facies metapelites from Southern Madagascar. Precamb. Res. 102, 47–68.

Martelat, J.-E., 1998. Evolution thermomécanique de la croûte inférieure du sud de Madagascar. Ph.D. thesis, Université Blaise Pascal, Clermont Ferrand.

Martelat, J.-E., Lardeaux, J.-M., Nicollet, C., Rakotondrazafy, R., 1999a. Exhumation of granulites within a transpressive regime: an example from southern Madagascar. Gondwana Res. 2, 363–368.

Martelat, J.-E., Lardeaux, J.-M., Nicollet, C., Rakotondrazafy, R., 2000. Strain pattern and late Precambrian deformation history in southern Madagascar. Precamb. Res. 102, 1–20.

Martelat, J.-E., Schulmann, K., Lardeaux, J.-M., Nicollet, C., Cardon, H., 1999b. Granulite microfabrics and deformation mechanisms in southern Madagascar. J. Struct. Geol. 21, 671–687.

Martelat, J.-E., Nicollet, C., Lardeaux, J.-M., Rakotondrazafy, R., 1997. Lithospheric tectonic structures developed under high-grade metamorphism in the Southern part of Madagascar. Geodin. Acta 10, 94–117.

Montel, J.M., Foret, S., Veschambre, M., Nicollet, C., Provost, A., 1996. Electron microprobe dating of monazite. Chem. Geol. 131, 37–53.

Nicollet, C., 1985. Les gneiss rubanés a cordiérite et grenat d'Ihosy: un marqueur thermobarométrque dans le Sud de Madagascar. Precamb. Res. 30, 175–185.

Nicollet, C., 1988, Métabasites granlitiques, anorthosites et roches associées de la croute inférieure. Exemples pris à Madagascar et dans le Massif Central français. Arguments en foveur d'un métamorphisme associé à l'extemsion lithosphérique: Unpubl. Thése d'Etat, Univ. Clermont-Ferrand, France, 315 pp.

Nicollet, C., 1990a. Crustal evolution of the granulites of Madagascar. In: Vielzeuf, D., Vidal, P. (Eds.), Granulites and Crustal Evolution, NATO ASI Series C: Mathematical and Physical Sciences. Kluwer, Dordrecht, pp. 219–310.

Nicollet, C., 1990b. Occurrences of grandidierite, serendibite and tourmaline near Ihosy, Southern Madagascar. Mineral. Mag. 54, 131–133.

Nicollet, C., Montel, J.M. Foret, J.E. Rakvotondrazafy, R., Lardeaux, J.M., 1997. Electron probe monazite dating in Madagascar: a good example of usefulness of the in situ dating method. In: Cox, R. Ashwal, L.D. (Eds.) Gondwana Research Group Misc. Publ. 5, pp. 65–66.

ORIGIN 6, 1999. Microcal Software Inc. Data analysis and technical graphics software. Microcal Software Inc. Northhampton, USA.

Paquette, J.-L., Nédélec, A., 1998. A new insight into Pan-African tectonics in the East–West Gondwana collision zone by U–Pb zircon dating of granites from central Madagascar. Earth Planet. Sci. Lett. 155, 45–56.

Paquette, J.-L., Moine, B., Rakotondrazafy, A.F., 2003. ID-TIMS using the step-wise dissolution technique vesus ion microprobe U–Pb dating of metamict Archean zircons from NE Madagscar. Precamb. Res. 121, 73–84.

Parrish, R.R., 1990. U–Pb dating of monazite and its application to geological problems. Can. J. Earth Sci. 27, 1431–1450.

Pili, E., Ricard, Y., Lardeaux, J.-M., Sheppard, S.M.F., 1997. Lithospheric shear zones and mantle-crust connections. Tectonophysics 280, 15–29.

Pyle, J.M., Spear, F.S., Rudnick, R.L., McDonough, W.F., 2001. Monazite-xenotime-garnet equilibrium in metapelites and a new monazite-garnet thermometer. J. Petrol. 42, 2083–2107.

Rolin, P., 1991. Présence de décrochements précambriens dans le bouclier méridional de Madagascar, Implications structurales et géodynamiques. C.R. Acad. Sci. Paris, Sér. II 312, 625–629.

Scherrer, N.C., Engi, M., Gnos, E., Jakob, V., Liechti, A., 2000. Monazite analysis; from sample preparation to microprobe age dating and REE quantification. Schweiz. Mineral. Petr. Mitt. 80, 93–105.

Tucker, R.D., Ashwal, L.D., Handke, M.J., Hamilton, M.A., LeGrange, M., Rambeloson, R.A., 1999. U–Pb geochronology and isotope geochemistry of the Archean and Proterozoic rocks of north-central Madagascar. J. Geol. Soc. Lond. 107, 135–153.

Vielzeuf, D., Schmidt, M.W., 2001. Melting relations in hydrous systems revisited: application to metapelites, metagreywackes and metabasalts. Contrib. Mineral. Petrol. 141, 251–267.

Windley, B.F., Razafiniparany, A., Razakamanana, T., Ackermand, D., 1994. Tectonic framework of the Precambrian of Madagascar and its Gondwana connections: A review and reappraisal. Geol. Rundsch. 83, 642–659.